Searching for new physics with di-boson measurements in ATLAS

Magdalena Sławińska

IFJ PAN, Kraków

Outline

- Motivation
  - searches for electroweak di-boson production
  - measurements of triple and quatric gauge boson couplings
  - searches for BSM physics in the framework of Standard Model Electroweak Field Theory (SMEFT)
- Vector Boson Scattering
  - two same-sign W bosons accompanied by two jets
  - Z boson pair and two jets
  - photon-induced production of W boson pairs
  - vector boson fusion Higgs production using decays to two W bosons
- Measurement of the four-lepton invariant mass spectrum
- Production of two W bosons and at least one jet

Vector boson scattering at the LHC

vector boson scattering

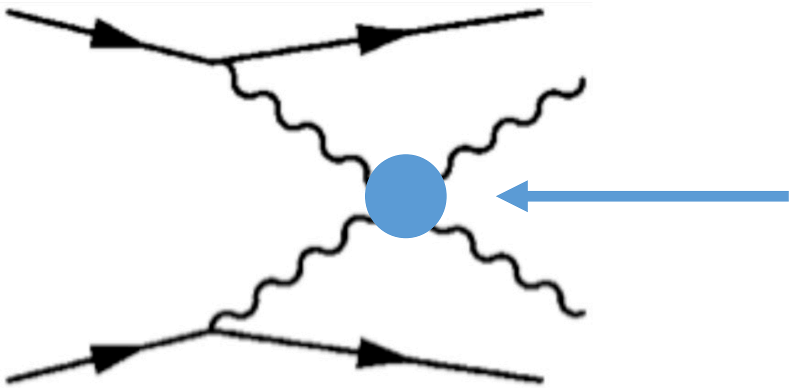

Motivation for VBF/VBS measurements

- couplings among gauge bosons as well as Higgs and gauge bosons precisely predicted in the SM
- EWK di-boson production at high energies is a sensitive probe of gauge (non-)cancellations that cause cross-sections to diverge
- probe of BSM (charged, composite, …) Higgs in its bosonic couplings

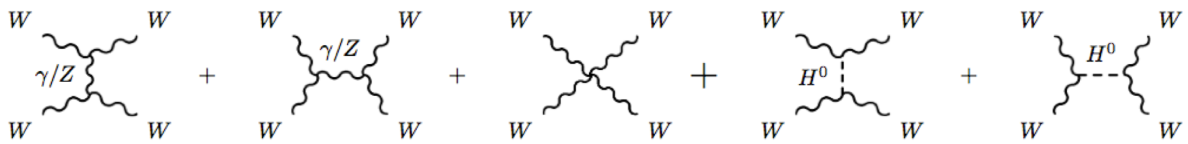

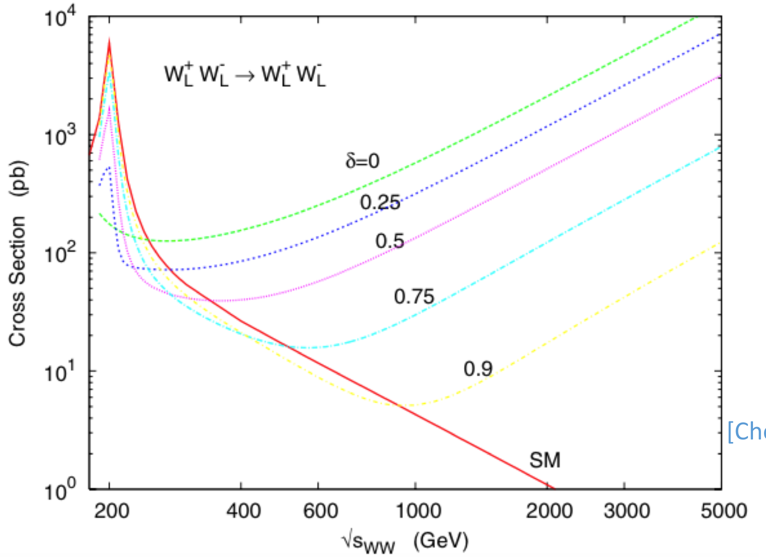

[Cheung, Chiang, Yuan, 2008]

Standard Model Effective Field Theory

- BSM fields above Λ=1TeV give rise to higher-dimensions operators that form SMEFT Lagrangian

$$L_{\text{EFT}} = L_{\text{SM}} + \sum_i \frac{\bar{C}_i^{(6)}}{\Lambda^2}\mathcal{O}_i^{(6)} + \sum_i \frac{\bar{C}_i^{(8)}}{\Lambda^4}\mathcal{O}_i^{(8)} + \dots \qquad (*)$$

- The canonical dimension of SM operators is 4, dim-6 operators suppressed by Λ^{-2} wrt. the SM, dim-8 operators suppressed by Λ^{-4} , …
- $C_i^{(d)}$ specify the strength of the BSM interactions and are known as Wilson coefficients, $c_i^{(6)} = C_i^{(6)} / \Lambda^{-2}$
- The set of operators of each dimension is renormalizable
- The complete basis of dim-6 operators is known JHEP10(2010) 085

(*) neglecting all lepton- and baryon-number violating terms, which include dim-5 operators

EFT cross-section measurements

- EFT dimension 6 operators implemented in the SMEFTSim package at the leading order
- Predicted cross-sections can be decomposed into:

$$\vec{\sigma}^{\text{pred}} = \vec{\sigma}^{\text{SM}} \times \left(1 + c_i \cdot \vec{\sigma}^{\text{INT}} / \vec{\sigma}^{\text{LO SM}} + c_i^2 \cdot \vec{\sigma}^{\text{BSM}} / \vec{\sigma}^{\text{LO SM}}\right)$$

- The linear (interference) and non-linear (quadratic) EFT contributions
- Quadratic term is of the same dimension as higher-order linear term thus some fit variants do not include it

Analysis strategy

- Select VVjj events
- Estimate non-VV processes from data
- Separate EWK processes from QCD interactions using kinematical properties:
  - forward high energetic jets with large separation in rapidity gap
  - large di-jet invariant mass
  - leptons central wrt. jets
- Measure EWK cross-section, (anomalous) couplings, EFT coefficients

EWK non-VBS

VBS di-boson production

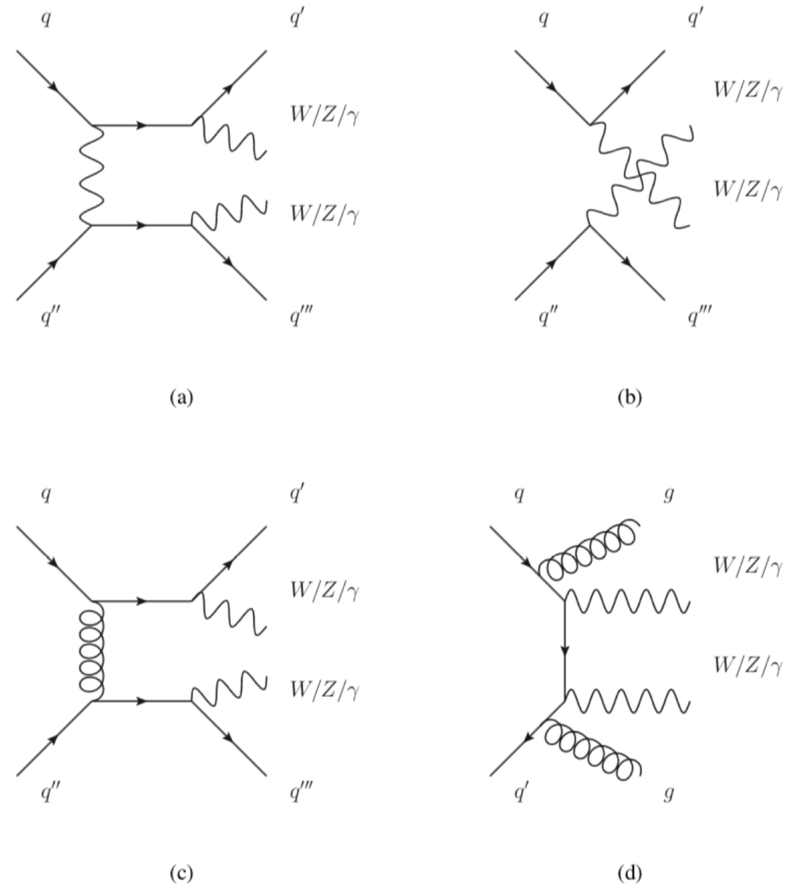

QCD production

1910.09503

Next To Leading Order cross-sections calculations

- LO contributions:
  - $\mathcal{O}(\alpha^6)$ EW
  - $\mathcal{O}(\alpha_s\alpha^5)$ interference
  - $\mathcal{O}(\alpha_s^2\alpha^4)$ QCD
- NLO contributions
  - $\mathcal{O}(\alpha^7)$ EW corrections
  - $\mathcal{O}(\alpha_s\alpha^6)$ QCD+EW
  - $\mathcal{O}(\alpha_s^2\alpha^5)$ QCD+EW
  - $\mathcal{O}(\alpha_s^3\alpha^4)$ QCD corrections

Beyond the leading order the distinction between EW and QCD contributions is meaningless.

Full NLO QCD+EW corrections available only for $W^\pm W^\pm j\, j$

State of the art of theory predictions:

- pure NLO QCD predictions computed for:
  - $W^\pm W^\pm j\, j$ (*)
  - $W^\pm Z$ jj (**)
  - ZZjj (***) and W^+W^- jj (****)
- pure NLO EW corrections computed for:
  - $W^\pm W^\pm j\, j$ (*)
  - $W^\pm Zjj$ (**)
- QCD+EW corrections:
  - $W^\pm W^\pm j\, j$ (*)
  - only $\mathcal{O}(\alpha_s\alpha^6)$ in $W^\pm Zjj$ (***), ZZjj (+) and W^+W^- jj (+ +)

(*) Biedermann, Denner, Pellen; 1611.02951, 1708.00268
(**) Denner, Dittmaier, Maierhoefer, Pellen, Schwan; 1904.00882
(***) Campanario et al.; 1305.1623
(****) Jaeger, Zanderighi; 1301.1695
(+) Jaeger, Karlberg, Zanderighi; 1312.3252
(+ +) Greiner et al.; 1202.6004

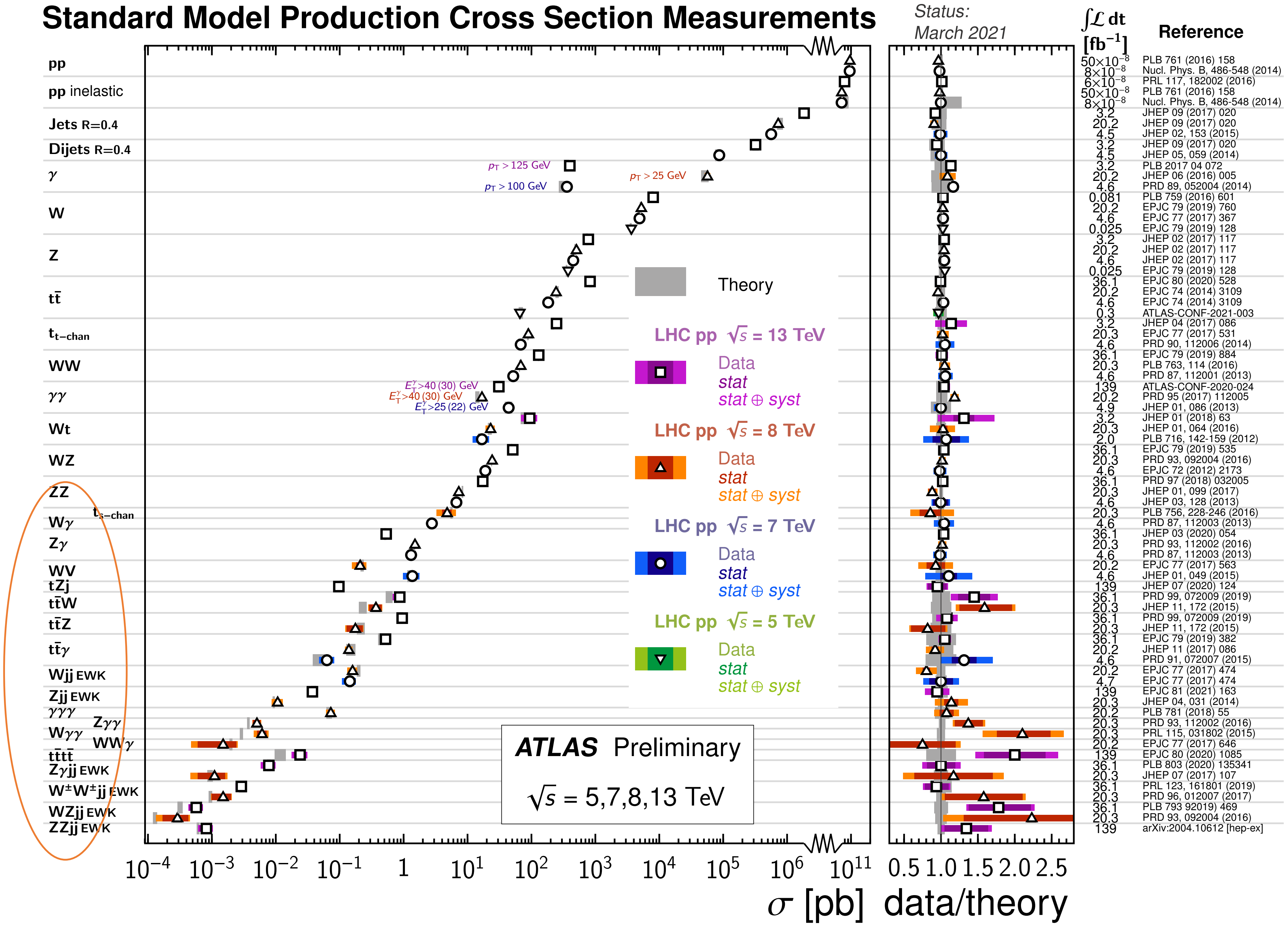
Standard Model Production Cross Section Measurements
Status: March 2021
∫ℒ dt [fb⁻¹]
Reference
pp
pp inelastic
Jets R=0.4
Dijets R=0.4
γ
W
Z
tt̄
t_t−chan
WW
γγ
Wt
WZ
ZZ
t_s−chan
Wγ
Zγ
WV
tZj
tt̄W
tt̄Z
tt̄γ
Wjj EWK
Zjj EWK
γγγ
Zγγ
Wγγ
WWγ
tt̄tt̄
Zγjj EWK
W±W±jj EWK
WZjj EWK
ZZjj EWK
p_T > 125 GeV
p_T > 100 GeV
p_T > 25 GeV
E_T^γ>40 (30) GeV
E_T^γ>40 (30) GeV
E_T^γ>25 (22) GeV
Theory
LHC pp √s = 13 TeV
Data
stat
stat ⊕ syst
LHC pp √s = 8 TeV
Data
stat
stat ⊕ syst
LHC pp √s = 7 TeV
Data
stat
stat ⊕ syst
LHC pp √s = 5 TeV
Data
stat
stat ⊕ syst
ATLAS Preliminary
√s = 5,7,8,13 TeV
10⁻⁴ 10⁻³ 10⁻² 10⁻¹ 1 10¹ 10² 10³ 10⁴ 10⁵ 10⁶ 10¹¹
σ [pb]
0.5 1.0 1.5 2.0 2.5
data/theory
50×10⁻⁸ PLB 761 (2016) 158
8×10⁻⁸ Nucl. Phys. B, 486-548 (2014)
6×10⁻⁸ PRL 117, 182002 (2016)
50×10⁻⁸ PLB 761 (2016) 158
8×10⁻⁸ Nucl. Phys. B, 486-548 (2014)
3.2 JHEP 09 (2017) 020
20.2 JHEP 09 (2017) 020
4.5 JHEP 02, 153 (2015)
3.2 JHEP 09 (2017) 020
4.5 JHEP 05, 059 (2014)
3.2 PLB 2017 04 072
20.2 JHEP 06 (2016) 005
4.6 PRD 89, 052004 (2014)
0.081 PLB 759 (2016) 601
20.2 EPJC 79 (2019) 760
4.6 EPJC 77 (2017) 367
0.025 EPJC 79 (2019) 128
3.2 JHEP 02 (2017) 117
20.2 JHEP 02 (2017) 117
4.6 JHEP 02 (2017) 117
0.025 EPJC 79 (2019) 128
36.1 EPJC 80 (2020) 528
20.2 EPJC 74 (2014) 3109
4.6 EPJC 74 (2014) 3109
0.3 ATLAS-CONF-2021-003
3.2 JHEP 04 (2017) 086
20.3 EPJC 77 (2017) 531
4.6 PRD 90, 112006 (2014)
36.1 EPJC 79 (2019) 884
20.3 PLB 763, 114 (2016)
4.6 PRD 87, 112001 (2013)
139 ATLAS-CONF-2020-024
20.2 PRD 95 (2017) 112005
4.9 JHEP 01, 086 (2013)
3.2 JHEP 01 (2018) 63
20.3 JHEP 01, 064 (2016)
2.0 PLB 716, 142-159 (2012)
36.1 EPJC 79 (2019) 535
20.3 PRD 93, 092004 (2016)
4.6 EPJC 72 (2012) 2173
36.1 PRD 97 (2018) 032005
20.3 JHEP 01, 099 (2017)
4.6 JHEP 03, 128 (2013)
20.3 PLB 756, 228-246 (2016)
4.6 PRD 87, 112003 (2013)
36.1 JHEP 03 (2020) 054
20.3 PRD 93, 112002 (2016)
4.6 PRD 87, 112003 (2013)
20.2 EPJC 77 (2017) 563
4.6 JHEP 01, 049 (2015)
139 JHEP 07 (2020) 124
36.1 PRD 99, 072009 (2019)
20.3 JHEP 11, 172 (2015)
36.1 PRD 99, 072009 (2019)
20.3 JHEP 11, 172 (2015)
36.1 EPJC 79 (2019) 382
20.2 JHEP 11 (2017) 086
4.6 PRD 91, 072007 (2015)
20.2 EPJC 77 (2017) 474
4.7 EPJC 77 (2017) 474
139 EPJC 81 (2021) 163
20.3 JHEP 04, 031 (2014)
20.2 PLB 781 (2018) 55
20.3 PRD 93, 112002 (2016)
20.3 PRL 115, 031802 (2015)
20.2 EPJC 77 (2017) 646
139 EPJC 80 (2020) 1085
36.1 PLB 803 (2020) 135341
20.3 JHEP 07 (2017) 107
36.1 PRL 123, 161801 (2019)
20.3 PRD 96, 012007 (2017)
36.1 PLB 793 92019) 469
20.3 PRD 93, 092004 (2016)
139 arXiv:2004.10612 [hep-ex]

in this talk

Experimental challenges in reconstructing forward objects

Jets

Jets reconstructed using AntiKT algorithm:

Small-R jets (R =0.4)

Large-R jets (R=1.0)

- to identify hadronically decaying boosted bosons
- p_T >200 GeV, $|\eta|<2$

Dedicated techniques to improve central jets reconstruction:

- JVT is applied to central jets with p_T < 60 GeV and $|\eta|$< 2.4 to suppress jets from pileup interactions.
- Two jet grooming definitions for reconstructing the Z→bb decay: trimming and soft drop.

Small-R jets selection in the central and forward region

Analysis\ min p_T	**$\|\eta\|$<2.5**	**2.5<$\|\eta\|$< 4.5**
semileptonic	20GeV	30GeV
$W^{\pm}W^{\pm}jj$	20GeV	25GeV
$Z\gamma$ jj	25 GeV	25 GeV
VBF H->WW	30 GeV	30 GeV

$$R = \sqrt{\Delta\eta^2 + \Delta\phi^2}$$

Tagging pileup jets in the forward region (fJVT)

- The dominant source of pileup in the forward region is QCD, while stochastic pile-up jets populate entire rapidity range
- track based jet vertex tagging (JVT) is limited to the tracker coverage $|\eta| < 2.4$
- calorimeter information available for jets $|\eta| < 4.9$
- The minimum $\Delta R p_T$ requirement defines the operating point in terms of hard-scatter and pileup efficiencies.

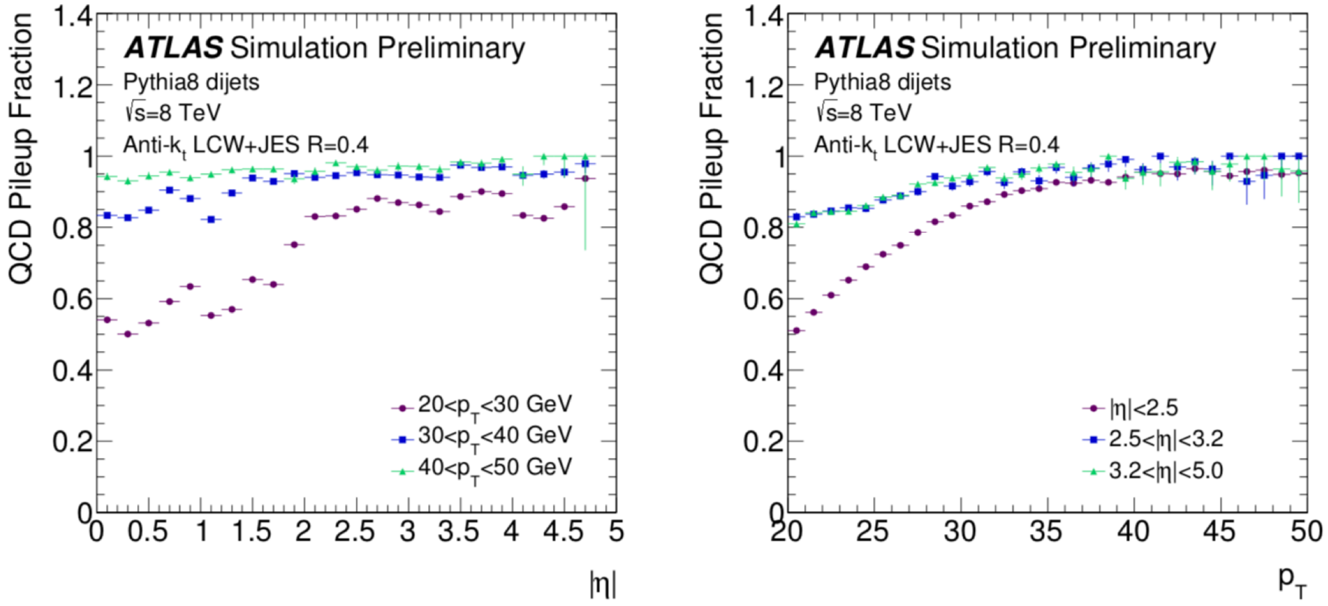

$$R_{\mathrm{pT}} = \frac{\sum_k p_{\mathrm{T}}^{\mathrm{trk}_k}(\mathrm{PV}_0)}{p_{\mathrm{T}}^{\mathrm{jet}}}.$$

Pileup in the forward region

- Applied in VBF H->WW(lvlv)
  - Tests in VBF H->WW using MCTruth information:
  - fJVT rejects 56% of events in which pile jet are taken as leading VBF jets, and 50% of events in which pile jet are taken as subleading VBF jets.
  - The VBF signal efficiency for the FJVT selection is about 76%
- used now also in EWK $W^{\pm}W^{\pm}jj$
- plans to use the fJVT tool before VBS jet selection in other EWK analyses

ATL-COM-PHYS-2017-1089

	bkg (no Wjets)	VBF signal
MVA> -0.8	758.96 ± 88.40	48.9 ± 0.59
lead jet is pileup	78.74 ± 25.00	0.13 ± 0.03
lead jet is pileup pass fJVT	44.76 ± 19.37	0.1 ± 0.02
lead jet is pileup pass fJVTTight	41.43 ± 19.35	0.1 ± 0.02

	bkg (no Wjets)	VBF signal
MVA> -0.8	758.96 ± 88.40	48.9 ± 0.59
lead jet is pileup	190.80 ± 36.34	1.17 ± 0.10
lead jet is pileup pass fJVT	101.84 ± 11.16	0.77 ± 0.09
lead jet is pileup pass fJVTTight	89.85 ± 10.79	0.63 ± 0.08

Jets containing heavy flavor quarks (b-jets)

- Flavour tagging used to suppress top backgrounds
- The chosen b-tagging algorithms vary in efficiency 70%-85%
- b-tagging only possible in central region |η| < 2.5, forward jets originating from top decays escape tagging

Analysis	b-tagging WP
$W^{\pm}W^{\pm}jj$	85%
ZZjj	85%
$Z\gamma$	70%
VBF H->WW	85%

Observation of electroweak same-sign W boson pairs accompanied by two jets

1906.03203

- The $W^{\pm}W^{\pm}jj$ final state has the largest ratio of electroweak to strong production cross sections compared to other VBS diboson processes
- integrated luminosity 36.1 fb^{-1}
- NLO QCD corrections included in EW and QCD $W^{\pm}W^{\pm}jj$
- The measured fiducial signal cross section is

$\sigma_{fid.}=2.89^{+0.51}_{-0.48}\,(stat.)\ ^{+0.29}_{-0.28}(syst.)$ fb.

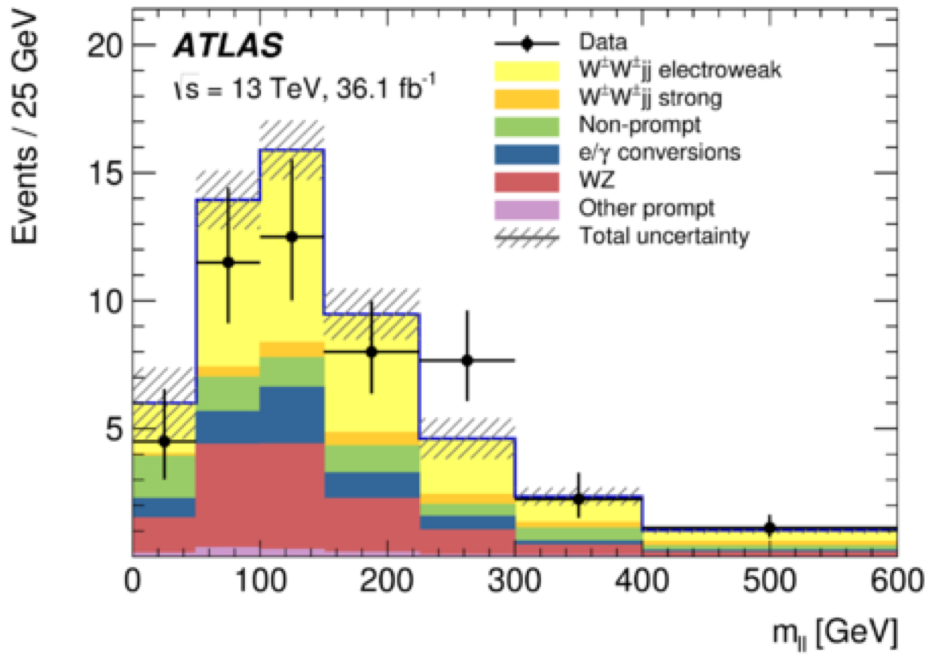

	e^+e^+	e^-e^-	$e^+\mu^+$	$e^-\mu^-$	$\mu^+\mu^+$	$\mu^-\mu^-$	Combined
WZ	1.48 ± 0.32	1.09 ± 0.27	11.6 ± 1.9	7.9 ± 1.4	5.0 ± 0.7	3.4 ± 0.6	30 ± 4
Non-prompt	2.2 ± 1.1	1.2 ± 0.6	5.9 ± 2.5	4.7 ± 1.6	0.56 ± 0.05	0.68 ± 0.13	15 ± 5
e/γ conversions	1.6 ± 0.4	1.6 ± 0.4	6.3 ± 1.6	4.3 ± 1.1	—	—	13.9 ± 2.9
Other prompt	0.16 ± 0.04	0.14 ± 0.04	0.90 ± 0.20	0.63 ± 0.14	0.39 ± 0.09	0.22 ± 0.05	2.4 ± 0.5
$W^{\pm}W^{\pm}jj$ strong	0.35 ± 0.13	0.15 ± 0.05	2.9 ± 1.0	1.2 ± 0.4	1.8 ± 0.6	0.76 ± 0.25	7.2 ± 2.3
Expected background	5.8 ± 1.4	4.1 ± 1.1	28 ± 4	18.8 ± 2.6	7.7 ± 0.9	5.1 ± 0.6	69 ± 7
$W^{\pm}W^{\pm}jj$ electroweak	5.6 ± 1.0	2.2 ± 0.4	24 ± 5	9.4 ± 1.8	13.4 ± 2.5	5.1 ± 1.0	60 ± 11
Data	10	4	44	28	25	11	122

Observation of electroweak production of two jets and a *Z*-boson pair

arXiv:2004.10612

- 2 final states: 4l jj and 2l2νjj
- integrated luminosity 139 fb^{-1}
- a fully reconstructed final state when both of the Z bosons decay into charged leptons
- VBS ZZ production is sensitive to the possible anomalous interaction between four Z bosons (forbidden at tree-level in the SM)

- small signal rate predicted by the SM, low background
- EW ZZjj signal generated at the LO, QCD-induced ZZjj production includes NLO QCD corrections
- Dominating sources of uncertainties are: data statics, experimental uncertainties related to jet measurements and the background estimate

Electroweak production of ZZjj

The hypothesis of no electroweak production is rejected with a statistical significance of 5.5σ, and the measured cross-section for electroweak production is consistent with the SM prediction.

signal strengths for QCD and EW production

	μ_{EW}	$\mu_{\mathrm{QCD}}^{\ell\ell\ell\ell jj}$	Significance Obs. (Exp.)
$\ell\ell\ell\ell jj$	1.5 ± 0.4	0.95 ± 0.22	$5.5\ (3.9)\ \sigma$
$\ell\ell\nu\nu jj$	0.7 ± 0.7	–	$1.2\ (1.8)\ \sigma$
Combined	1.35 ± 0.34	0.96 ± 0.22	$5.5\ (4.3)\ \sigma$

	Measured fiducial σ [fb]	Predicted fiducial σ [fb]
$\ell\ell\ell\ell jj$	$1.27 \pm 0.12(\mathrm{stat}) \pm 0.02(\mathrm{theo}) \pm 0.07(\mathrm{exp}) \pm 0.01(\mathrm{bkg}) \pm 0.03(\mathrm{lumi})$	$1.14 \pm 0.04(\mathrm{stat}) \pm 0.20(\mathrm{theo})$
$\ell\ell\nu\nu jj$	$1.22 \pm 0.30(\mathrm{stat}) \pm 0.04(\mathrm{theo}) \pm 0.06(\mathrm{exp}) \pm 0.16(\mathrm{bkg}) \pm 0.03(\mathrm{lumi})$	$1.07 \pm 0.01(\mathrm{stat}) \pm 0.12(\mathrm{theo})$

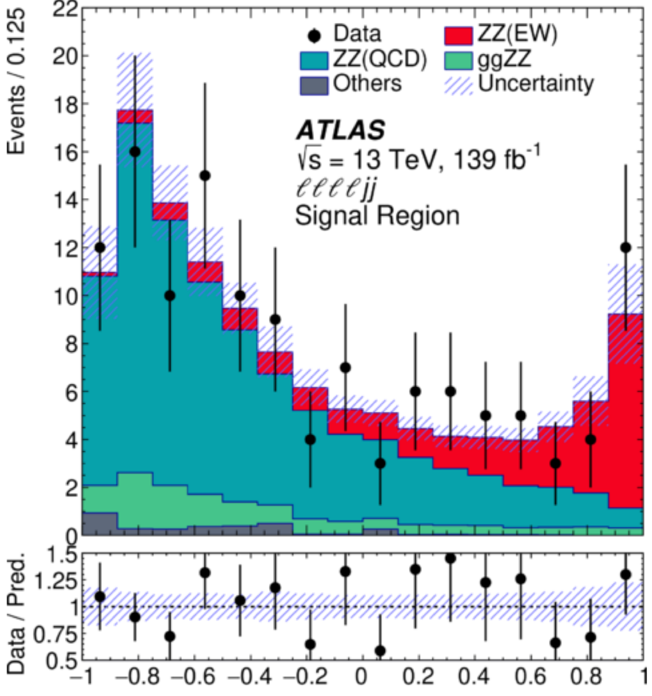

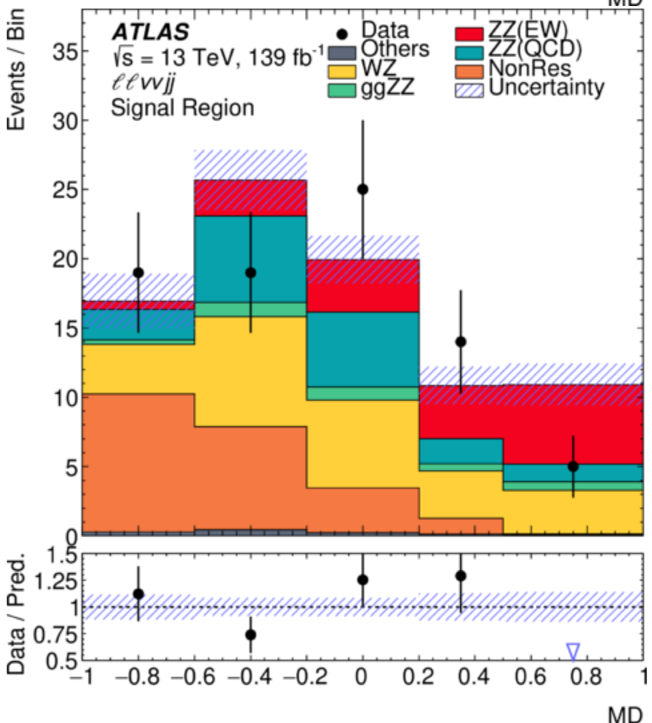

Observation of photon-induced production of W boson pairs

Elastic process

Inelastic process single dissociation

Inelastic process double dissociation

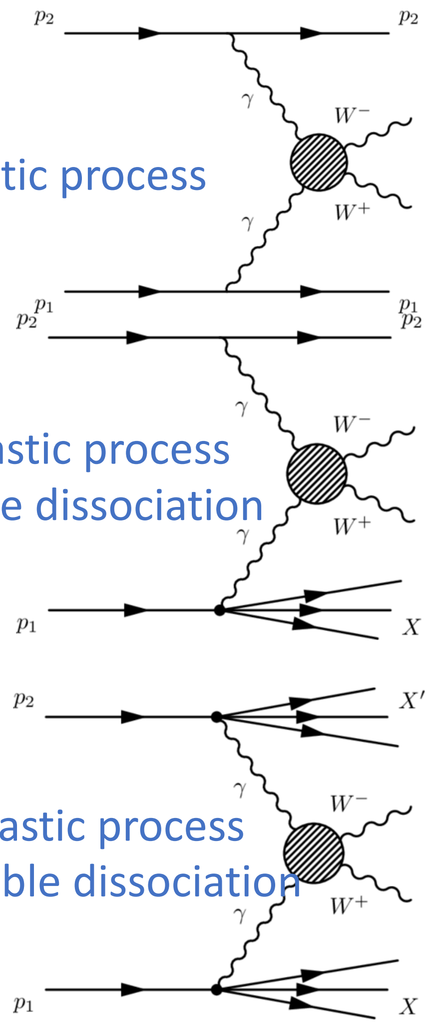

The signal is sensitive to triple and quartic gauge boson couplings

In the signal events the number of charged particles tracks is expected to be 0

- Modeling of hadronic activity is constrained using Drell-Yan events in data
- Observed significance of 6.7 standard deviations
- • Measured cross section:

$$3.13 \pm 0.31(\text{stat.}) \pm 0.28(\text{syst.})\ \text{fb}$$

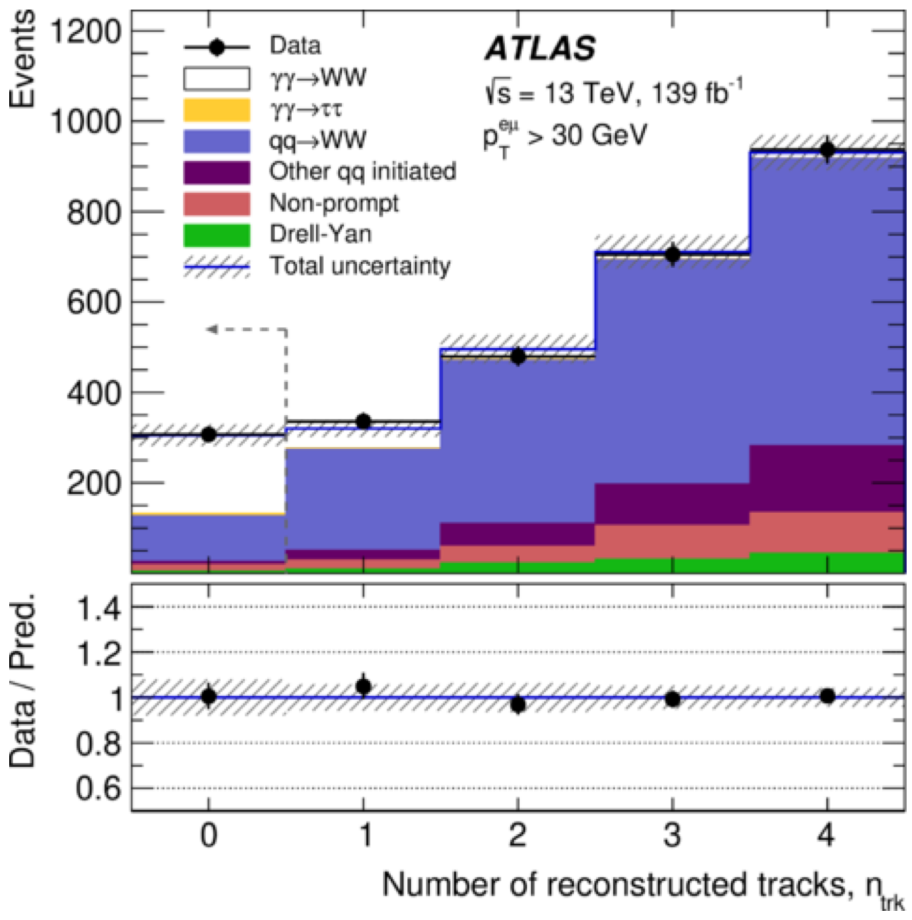

Constraining the Higgs boson couplings to longitudinally and transversally polarised W and Z bosons

- Vector boson fusion Higgs production and WW final state
- Integrated luminosity of 36 fb^{-1}
- $a_L = g_{HVLVL}/g_{HVV}$ and $a_T = g_{HVTVT}/g_{HVV}$,
  - in the SM $a_L = a_T = 1$
  - defined in the Higgs rest frame so that only HV_LV_L and HV_TV_T coupling combinations are present (see 1404.5951)

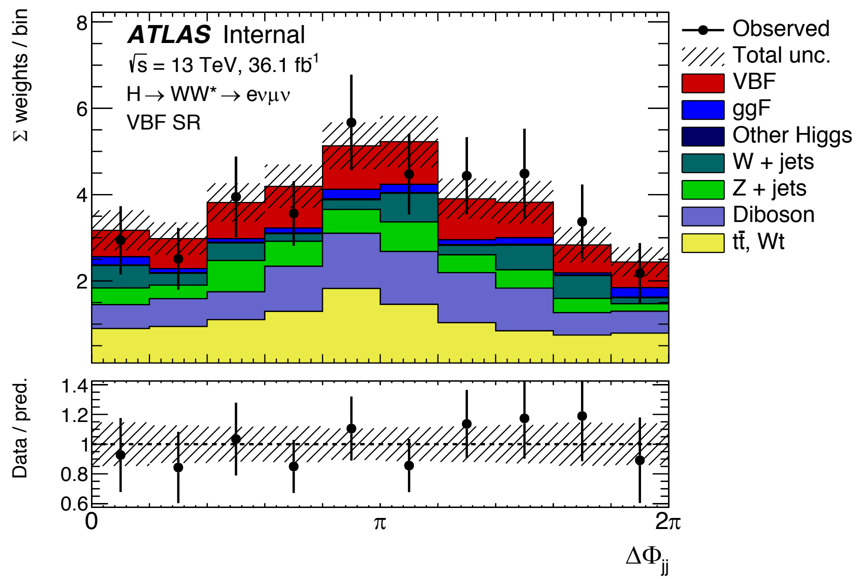

- Anomalous couplings extracted from:
- $\sigma \cdot Br(H \to WW^*)$
- the distribution of the signed azimuthal angle between two tagging jets $\Delta\Phi_{jj}$

Type	exp.	obs.
a_L shape-only fit ($a_T = 1$)	–	–
a_T shape-only fit ($a_L = 1$)	1.00 ± 0.5(stat.)$^{+0.35}_{-0.39}$(syst.)	$1.27^{+0.8}_{-0.4}$(stat.)$^{+0.35}_{-0.27}$(syst.)
a_L shape + rate fit ($a_T = 1$)	$1.00^{+0.08}_{-0.10}$(stat.)$^{+0.08}_{-0.13}$(syst.)	$0.90^{+0.10}_{-0.13}$ (stat.)$^{+0.09}_{-0.19}$(syst.)
a_T shape + rate fit ($a_L = 1$)	$1.00^{+0.36}_{-0.49}$(stat.)$^{+0.22}_{-0.32}$(syst.)	$1.18^{+0.26}_{-0.31}$(stat.)$^{+0.14}_{-0.16}$(syst.)
a_L shape + rate fit (a_T profiled)	$1.00^{+0.08}_{-0.10}$(stat.)$^{+0.08}_{-0.13}$(syst.)	$0.91^{+0.10}_{-0.18}$(stat.)$^{+0.09}_{-0.18}$(syst.)
a_T shape + rate fit (a_L profiled)	$1.00^{+0.38}_{-0.5}$(stat.)$^{+0.22}_{-0.43}$(syst.)	1.16 ± 0.4(stat.)$^{+0.4}_{-0.3}$(syst.)

di-boson measurements

Measurement of the four-lepton invariant mass spectrum

- The integrated luminosity of 139 fb^{-1}
- Selected events contain two same-flavour opposite-sign lepton pairs.
- Measurements of differential cross-section in the invariant four-lepton mass m_{4l},
- Measurements of double-differential cross-sections with respect to both m_{4l} and the following kinematic variables:
  - the transverse momentum of the four-lepton system p_{4l},
  - the rapidity of the four-lepton system y_{4l},
  - and a matrix-element discriminant DME

Measurement of the four-lepton invariant mass spectrum

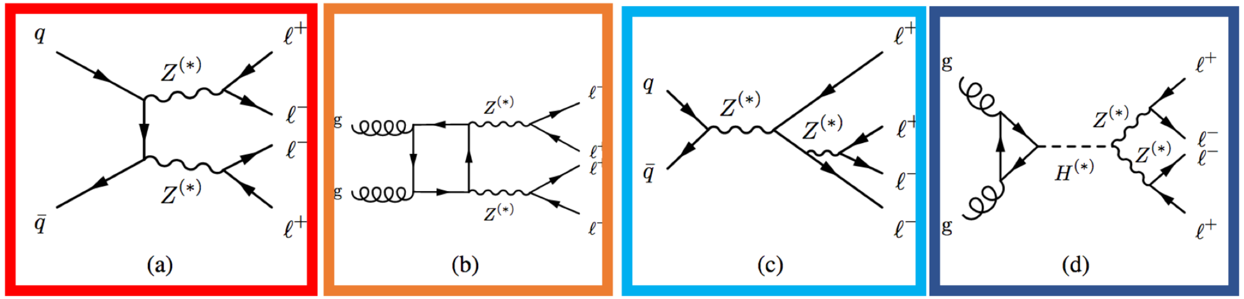

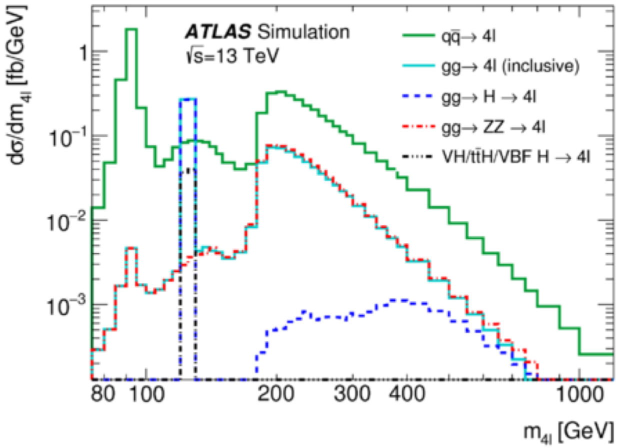

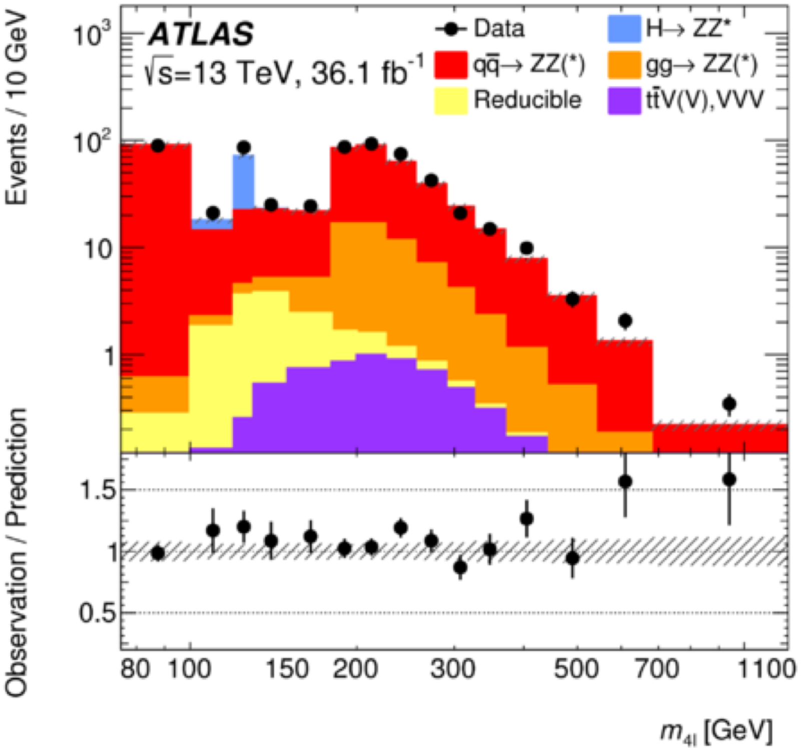

The final state has contributions from a number of processes that dominate in different four-lepton invariant mass regions.

measurement of Z→4l branching fraction

Extracted from the measured fiducial cross-section in the mass bin corresponding to m_Z

Measurement	$\mathcal{B}_{Z\to 4\ell}/10^{-6}$
ATLAS, $\sqrt{s} = 7$ TeV and 8 TeV [8]	$4.31 \pm 0.34(\text{stat}) \pm 0.17(\text{syst})$
CMS, $\sqrt{s} = 13$ TeV [6]	$4.83\ ^{+0.23}_{-0.22}(\text{stat})\ ^{+0.32}_{-0.29}(\text{syst}) \pm 0.08(\text{theo}) \pm 0.12(\text{lumi})$
ATLAS, $\sqrt{s} = 13$ TeV	$\mathbf{4.70 \pm 0.32(stat) \pm 0.21(syst) \pm 0.14(lumi)}$

Higgs boson measurements using 4 lepton invariant mass

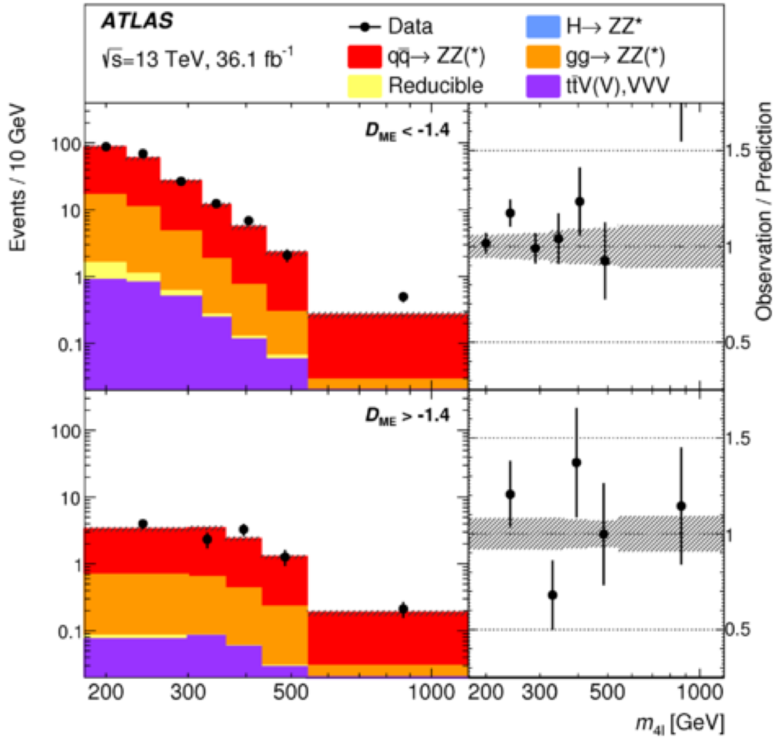

- Constraint on off-shell Higgs boson signal strength

-> from double-differential cross-section measured as a function of m_{4l} and the matrix element discriminant D_{ME},

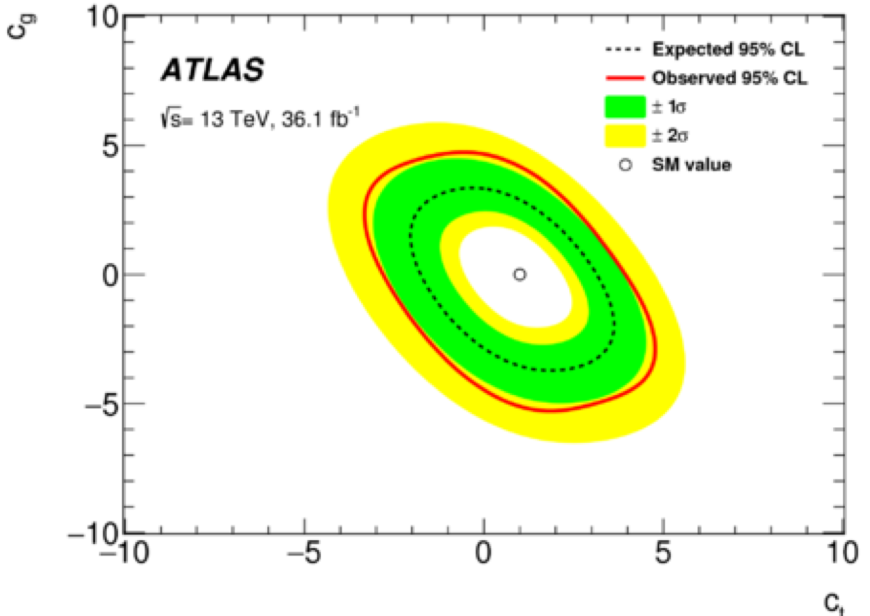

- Constraints to tree level Higgs couplings to top quarks (c_t) and to gluons (c_g)

-> from the measured differential cross-section as a function of m_{4l}.

On-shell rates for Higgs production via gluon–gluon fusion are only sensitive to $|ct+cg|^2$, but measurements at higher mass (>180GeV) can be used to probe these parameters independently

Constraints on EFT Wilson coefficients

operators affecting:

Higgs-gauge bosons couplings

gauge bosons couplings

Z→ll vertex

four-fermion contact terms

Only linear term included in the fit (non-linear variant included in the paper as well)

Coefficient	Observable	95% CL Expected [TeV^{-2}]	95% CL Observed [TeV^{-2}]
c_{HG}	m_{34} vs $m_{4\ell}$	$[-0.011, 0.013]$	$[-0.0090, 0.014]$
$\tilde{c}_{HG}$	m_{34} vs $m_{4\ell}$	–	–
c_{HD}	m_{34} vs $m_{4\ell}$	$[-0.46, 0.44]$	$[-0.63, 0.28]$
c_{HWB}	m_{34} vs $m_{4\ell}$	$[-0.21, 0.20]$	$[-0.29, 0.13]$
c_{Hd}	$p_{T,12}$ vs $m_{4\ell}$	$[-10, 10]$	$[-3.0, 18]$
c_{Hu}	$\lvert\Delta\phi_{\ell\ell}\rvert$ vs $m_{4\ell}$	$[-3.5, 3.7]$	$[-1.6, 6.2]$
c_{He}	$\lvert\Delta\phi_{\text{pairs}}\rvert$ vs $m_{4\ell}$	$[-0.48, 0.46]$	$[-0.76, 0.21]$
$c_{Hl}^{(1)}$	$\lvert\Delta\phi_{\text{pairs}}\rvert$ vs $m_{4\ell}$	$[-0.37, 0.38]$	$[-0.19, 0.57]$
$c_{Hl}^{(3)}$	$\lvert\Delta\phi_{\ell\ell}\rvert$ vs $m_{4\ell}$	$[-0.29, 0.28]$	$[-0.51, 0.12]$
$c_{Hq}^{(1)}$	m_{34} vs $m_{4\ell}$	$[-0.81, 0.78]$	$[-1.1, 0.46]$
$c_{Hq}^{(3)}$	$\lvert\Delta\phi_{\text{pairs}}\rvert$ vs $m_{4\ell}$	$[-0.34, 0.33]$	$[-0.15, 0.54]$
c_{ed}	m_{34} vs $m_{4\ell}$	$[-1.3, 1.8]$	$[-0.98, 2.3]$
c_{ee}	m_{34} vs $m_{4\ell}$	$[-58, 64]$	$[-27, 100]$
c_{eu}	$m_{4\ell}$	$[-0.61, 0.45]$	$[-0.36, 0.64]$
c_{ld}	m_{34} vs $m_{4\ell}$	$[-1.8, 2.5]$	$[-1.4, 3.0]$
c_{le}	m_{34} vs $m_{4\ell}$	$[-63, 68]$	$[-18, 130]$
c_{ll}	m_{34} vs $m_{4\ell}$	$[-39, 43]$	$[-17, 71]$
$c_{ll}^{(1)}$	$\lvert\Delta\phi_{\text{pairs}}\rvert$ vs $m_{4\ell}$	$[-0.33, 0.34]$	$[-0.17, 0.51]$
$c_{lq}^{(1)}$	$m_{4\ell}$	$[-0.77, 0.40]$	$[-4.1, 0.55]$
$c_{lq}^{(3)}$	m_{34} vs $m_{4\ell}$	$[-0.061, 0.083]$	$[-0.051, 0.098]$
c_{lu}	$m_{4\ell}$	$[-1.4, 0.98]$	$[-0.77, 1.4]$
c_{qe}	$m_{4\ell}$	$[-1.1, 0.84]$	$[-0.67, 1.2]$

Arxiv:2103.10319

WW+jets

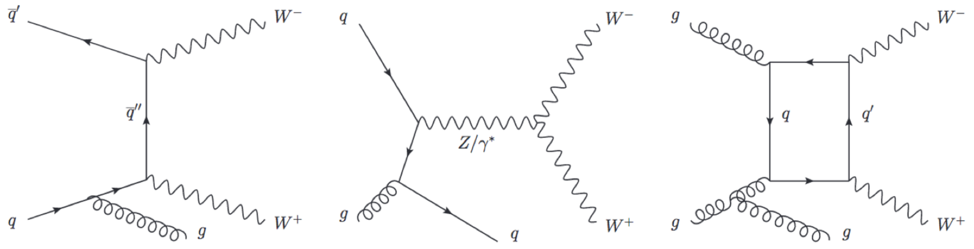

WW+j production

Fiducial selection requirements		
p_T^ℓ	>	27 GeV
$\lvert\eta^\ell\rvert$	<	2.5
$m_{e\mu}$	>	85 GeV
p_T^j	>	30 GeV
$\lvert y^j\rvert$	<	4.5

- The WW+jets cross-section is evaluated in the fiducial phase space of the $WW \rightarrow e\nu\mu\nu$ decay channel
- at least one jet required in the event selection
- Background estimation:
  - Top quark: ttbar from CR, Wt from simulation
  - Drell-Yan from MC (validation region)
  - Fake-lepton backgrounds estimated using a data-driven technique
  - Backgrounds from WZ, ZZ, $W\gamma$ and $Z\gamma$ from simulation
  - triboson background neglected

WW+jets

- The differential cross-sections are determined using an iterative Bayesian unfolding method and compared to numerous theory predictions

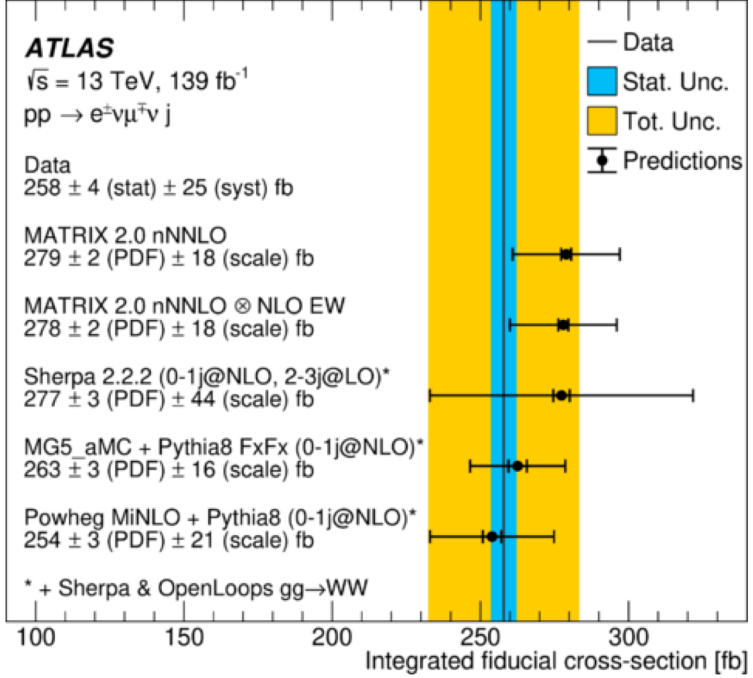

- Fiducial cross-section and differential cross-section with respect to several kinematical variables related to leptons and jets are measured

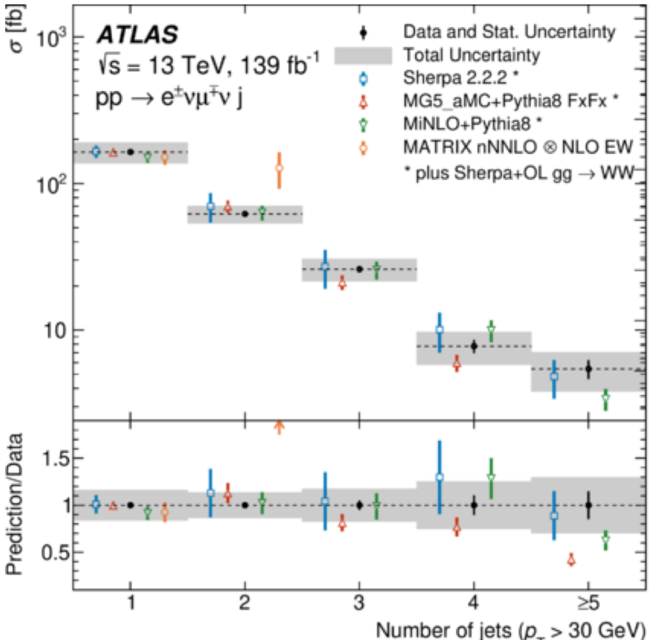

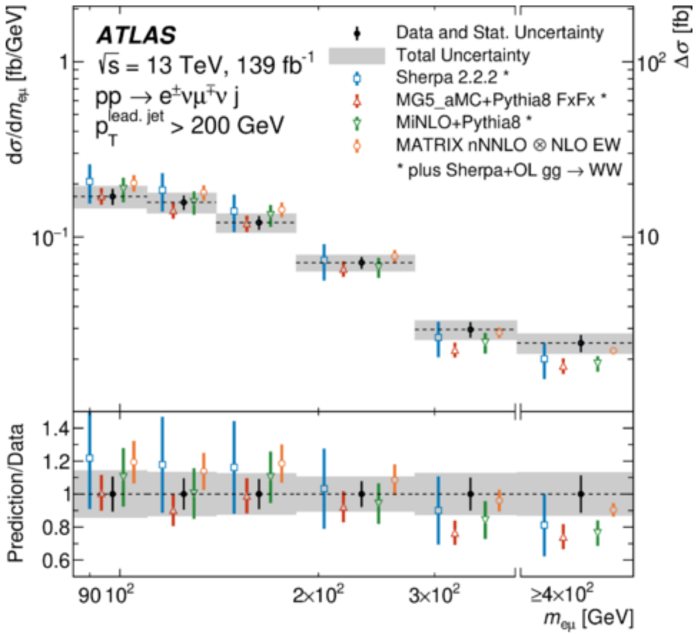

WW+ jets

- Limits set on anomalous triple gauge couplings
- Limits set on a single EFT parameter c_W
- Interference between the Standard Model amplitude and the anomalous amplitude enhanced by kinematical selection (p_T^j> 200 GeV)

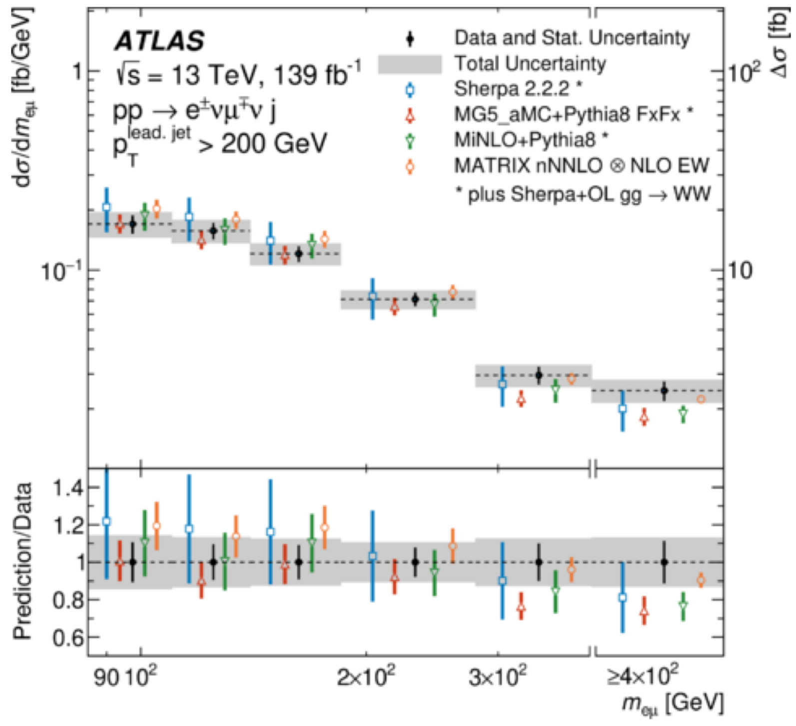

Table 8: Observed and expected confidence intervals (CI) for c_W for a linearized and a quadratic EFT fit of $m_{e\mu}$, when requiring either jet $p_T > 30$ GeV or jet $p_T > 200$ GeV. The new-physics scale Λ is set to 1 TeV.

Jet p_T	Linear only	68% CI obs.	95% CI obs.	68% CI exp.	95% CI exp.
> 30 GeV	yes	[–1.64, 2.86]	[–3.85, 4.97]	[–2.30, 2.27]	[–4.53, 4.41]
> 30 GeV	no	[–0.20, 0.20]	[–0.33, 0.33]	[–0.28, 0.27]	[–0.39, 0.38]
> 200 GeV	yes	[–0.29, 1.84]	[–1.37, 2.81]	[–1.12, 1.09]	[–2.24, 2.10]
> 200 GeV	no	[–0.43, 0.46]	[–0.60, 0.58]	[–0.38, 0.33]	[–0.53, 0.48]

Di-Higgs measurements

Di-Higgs production in the SM and the trilinear coupling (+BSM searches)

2014 projection vs results of early 2015+16 combination

update on bblνlν (inclusion of 3 channels)

Electroweak Symmetry Breaking in the SM

- The SM Higgs potential

$$V = -\mu H^2 + \lambda H^4$$

EWSB

$$V = \frac{m_h^2}{2} h^2 + \lambda_3 v h^3 + \frac{\lambda_4}{4} h^4$$

$m_h^2 = \lambda v^2$

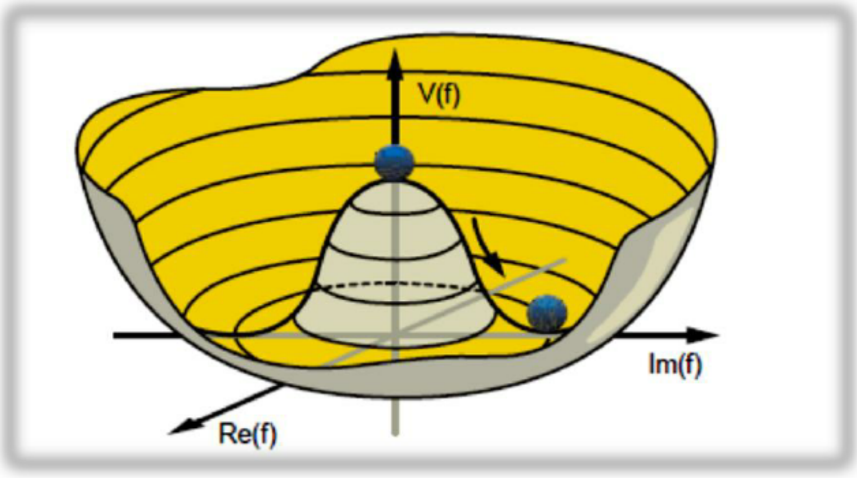

$$\lambda_3 = \lambda_4 = m_h^2/(2v^2)$$

Higgs triple and quadruple self-couplings

A different electroweak symmetry breaking mechanism would result in a different shape of the Higgs potential.

The shape of the Higgs potential

Measuring its couplings to bosons and fermions ↔ properties of the Higgs potential close to the vacuum.

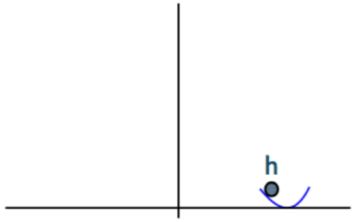

from 1511.06495

The shape of the Higgs potential

Measuring its couplings to bosons and fermions ↔ properties of the Higgs potential close to the vacuum.

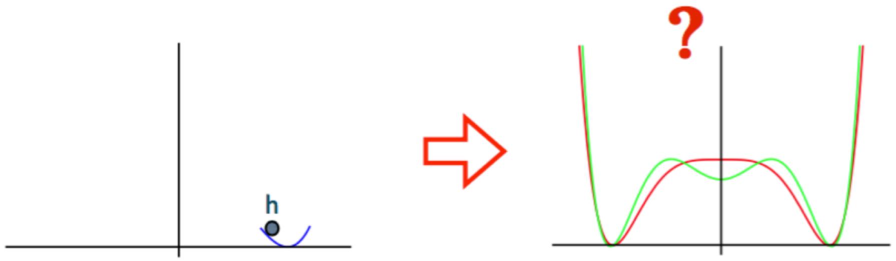

from 1511.06495

- But... the potential can be different, even non-analytic!

$$V(h) \to \frac{1}{2}\lambda(h^\dagger h)^2 \log\left[\frac{(h^\dagger h)}{m^2}\right].$$

Phys.Rev. D7 (1973) 1888–1910

The shape of the Higgs potential

Measuring its couplings to bosons and fermions ↔ properties of the Higgs potential close to the vacuum.

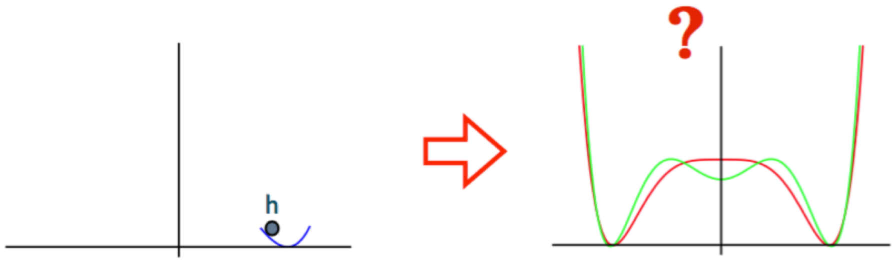

from 1511.06495

- But... the potential can be different, even non-analytic!

$$V(h) \to \frac{1}{2}\lambda(h^\dagger h)^2 \log\left[\frac{(h^\dagger h)}{m^2}\right].$$

Phys.Rev. D7 (1973) 1888–1910

- Leading differences among various potentials are visible in the value of the Higgs self-couplings. In general, both self-couplings can differ.

- Higgs triple-interactions can be probed directly by di-Higgs production processes.

Di-Higgs production channels in the SM

3 orders
of magnitude
wrt. single Higgs
production

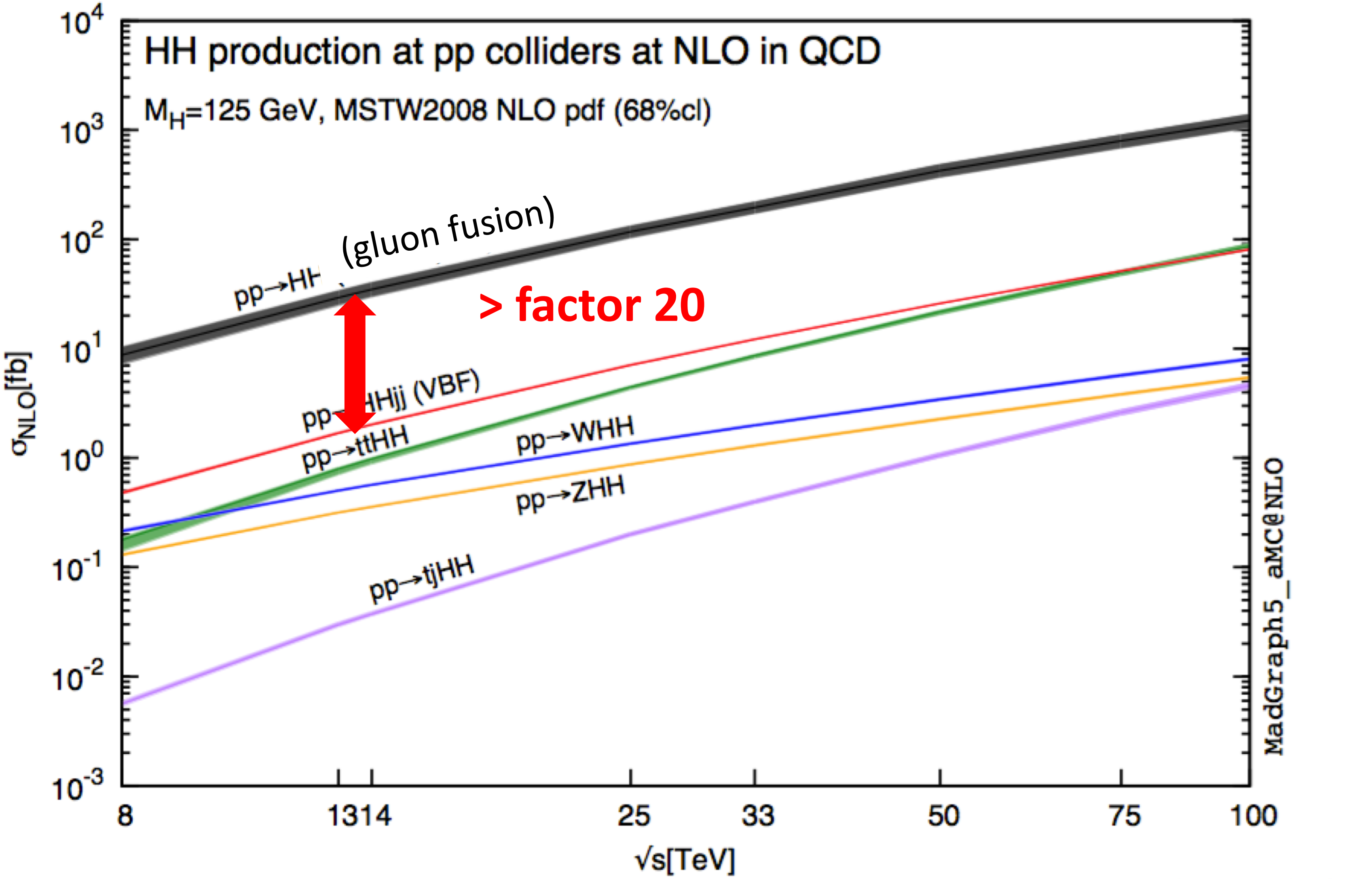

[Frederix et al ` 14]

Cross-section calculations

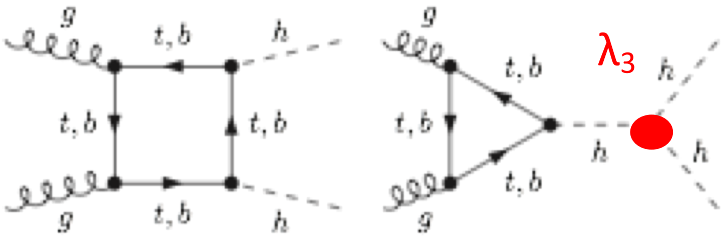

Di Higgs production is loop induced already at the leading order.

- LO

  [Glover, van der Bij `88] [Plehn, Spira, Zerwas `96] [Djouadi et al `99] …

- NLO ($m_t \to \infty$)

  [Dawson, Dittmaier, Spira `98] [de Florian, Mazzitelli `13]

- NNLO+NNLL in $m_t \to \infty$ (Born normalised to exact LO)

  [de Florian, Mazzitelli `13, `15]

- exact m_t for real emission & LO reweighted virtuals

  [Frederix et al `14] [Maltoni, Vryonidou, Zaro `14]

- NLO

  [Borowka, Greiner, Heinrich, Jones, MK, Schlenk, Schubert, Zirke `16]

gg → hh kinematics

arXiv:1408:5010

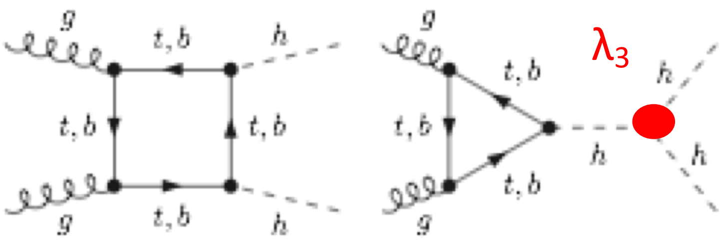

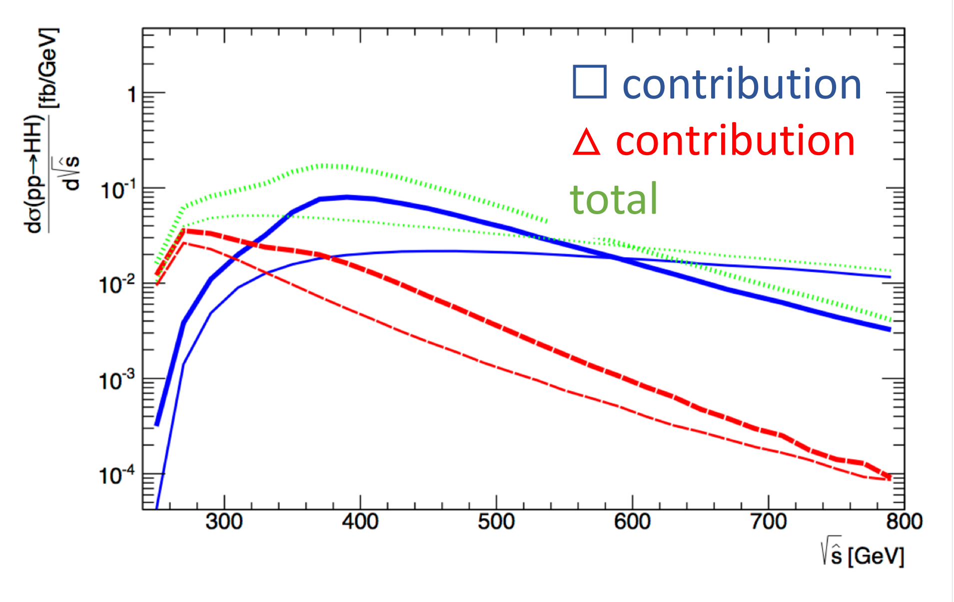

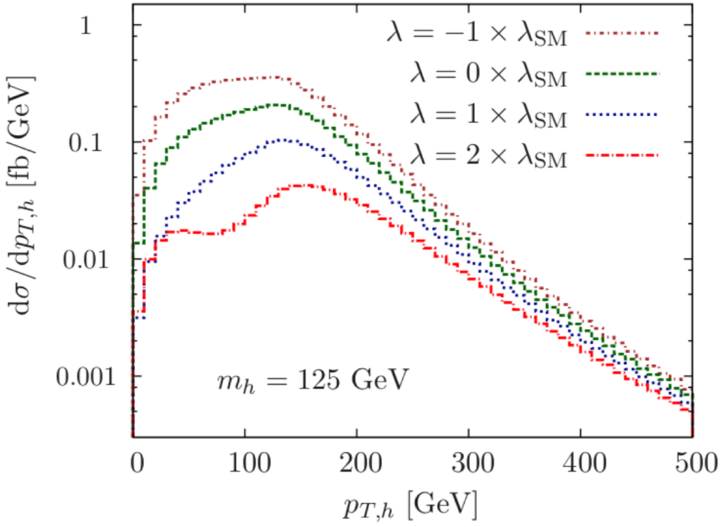

- The Higgs self-coupling contribution small due to Higgs propagators.
- Negative interference between both diagrams results in small total cross-section.
- Kinematics of the process depends on λ_3.

Expected numbers of di-Higgs events at the LHC

Final state	Branching ratios	N Run 1 ($L=20\ fb^{-1}$)	N Run 2 ($L=36\ fb^{-1}$)	N HL-LHC ($L=3000\ fb^{-1}$)
bbbb	34%	**76**	463	45841
bb WW(lvlv)	25%(0.3%)	56 (0.6)	340 (3.9)	33641 (383)
bbττ	4%	**8**	50	4937
bbZZ (lvlv)	3%(0.1%)	6.8 (0.2)	41.7 (1.1)	4123 (111)
bbγγ	0.3%	**1**	4	357
γγWW(lvjj)	0.1%(0.03%)	**0**	1(0.4)	131(38)

LHCHXSWG YR4, arXiv:1610.07922v2,
based on: arXiv:1505.07122, arXiv:1604.06447

Prospects for measuring Higgs pair production in the channel $H(\rightarrow\gamma\gamma)H(\rightarrow bb)$ using the ATLAS detector at the HL-LHC

ATL-PHYS-PUB-2014-019

- Projections made in 2014 using fast simulation of the upgraded detector performance
- The expected number of background events is ∼47 and signal events is ~8, corresponding to a signal significance of 1.3 σ.
  - cut-based event selection
  - optimistic assumptions about pileup
  - rough estimate of flavor tagging performance
  - pessimistic assumptions of detector coverage
- systematical uncertainties not included
- Overall projected sensitivity much worse than assumed by theorists mainly due to momentum resolution of reconstructed particles.

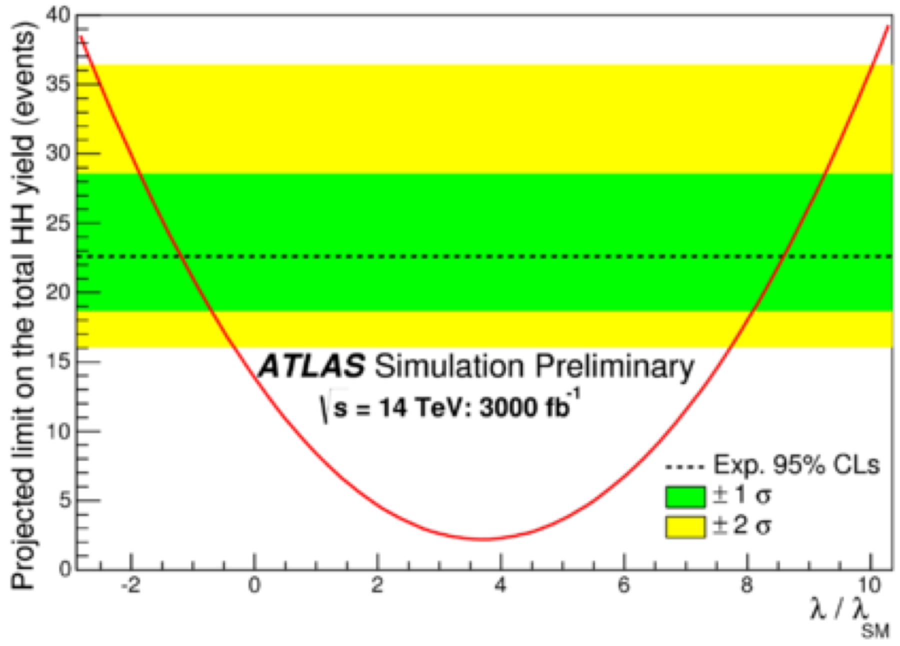

exclusion at 95% C.L.
$\lambda/\lambda_{SM} < -1.3$ and $\lambda/\lambda_{SM} < 8.7$.

Search for Higgs boson pair production in the bbγγ final state

JHEP 11 (2018) 040

- pp collision data at √s=13 TeV
- integrated luminosity of 36.1/fb
- Selection requirements:
  - two isolated photons
  - two jets whose invariant mass is compatible with the Higgs mass
  - 1 or 2 jets are tagged as b-jets
  - loose and tight kinematic selections defined (b-tagging efficiency, jets requirements and m_{jj} window)
- Signal extracted using a fit to the diphoton invariant mass distribution of the selected events.
- The Higgs boson self-coupling is constrained at 95% CL to $-8.2 < \lambda_{HHH}/\lambda^{SM}_{HHH} < 13.2$

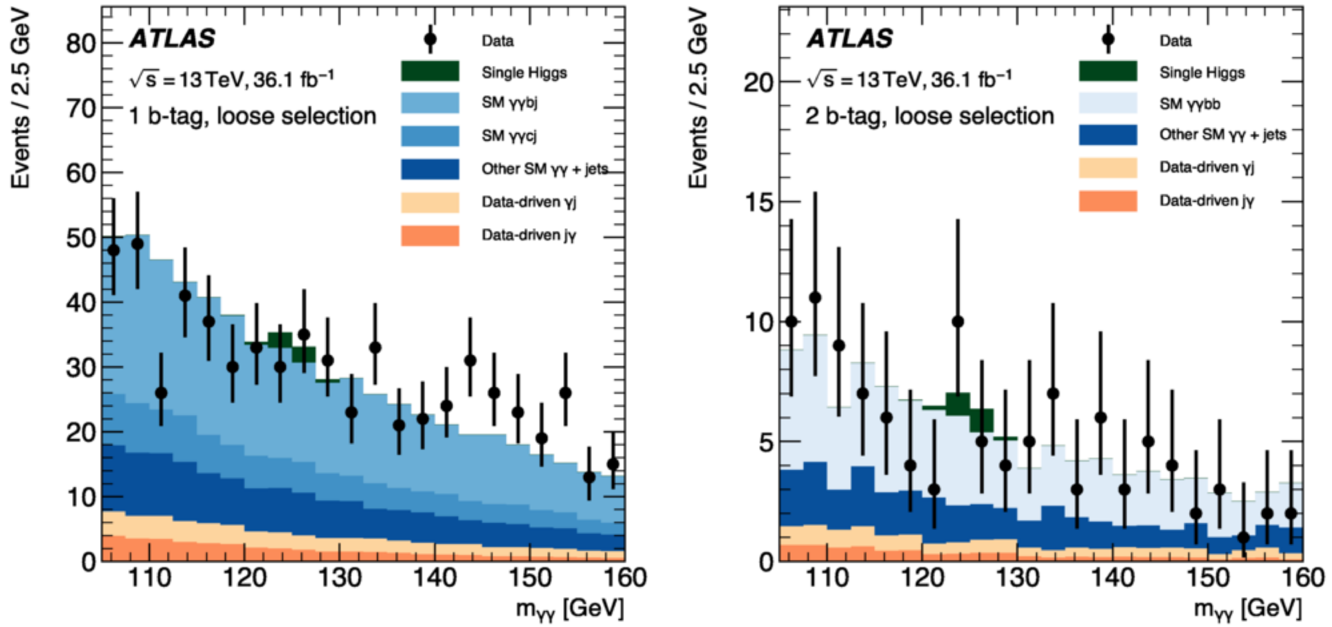

Search for Higgs boson pair production in the bbγγ final state

Limits on a BSM electroweak singlet

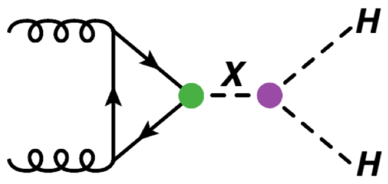

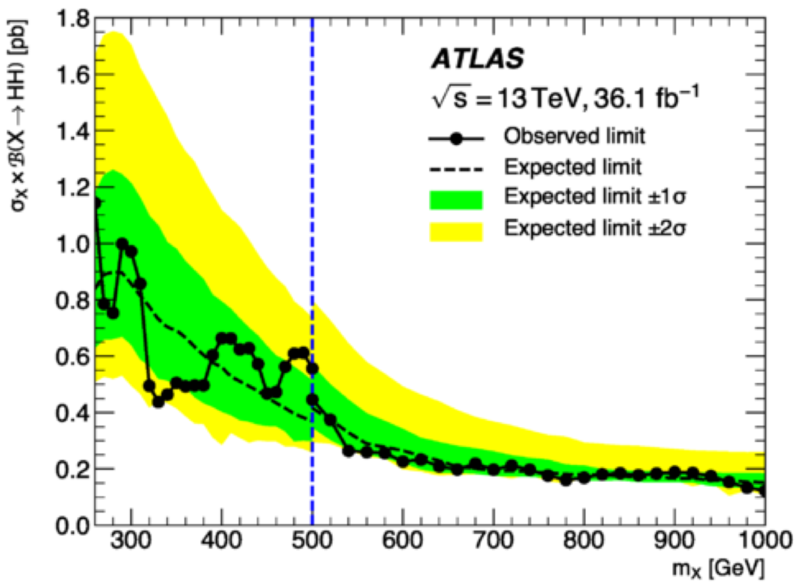

- Additional di-Higgs production mechanism through an electroweak singlet X.
- The signal is extracted from the four-object invariant mass ($m_{\gamma\gamma jj}$) spectrum by fitting a resonance peak superimposed on a smoothly changing background.
- The narrow-width approximation is used, probing the range the range 260 GeV<m_X<1000 GeV.
- Loose selection is used for resonances with $m_X \leq$ 500 GeV and the tight selection for resonances with $m_X \geq$ 500 GeV

2019 combination

Phys. Lett. B 800 (2020) 135103

- Combination of 6 analyses
  - pp collision data at √s=13 TeV
  - integrated luminosity of 36.1/fb

	$b\bar{b}b\bar{b}$	$b\bar{b}W^+W^-$	$b\bar{b}\tau^+\tau^-$	$W^+W^-W^+W^-$	$b\bar{b}\gamma\gamma$	$W^+W^-\gamma\gamma$
$\mathcal{B}(HH \to x\bar{x}y\bar{y})$	0.34	0.25	0.073	0.046	$2.6 \cdot 10^{-3}$	$1.0 \cdot 10^{-3}$
$\mathcal{L}_{\text{int}}$ [fb^{-1}]	27.5 [36.1]	36.1	36.1	36.1	36.1	36.1
Categories	2 [2–5]	1 [1]	3 [2–3]	9 [9]	2 [2]	1 [1]
Discriminant	m_{HH} [m_{HH}]	c.e. [m_{HH}]	BDT [BDT]	c.e. [c.e.]	$m_{\gamma\gamma}$ [m_{HH}]	$m_{\gamma\gamma}$ [$m_{\gamma\gamma}$]
Model	NR [S/G]	NR [S/G]	NR [S/G]	NR [S]	NR [S]	NR [S]
$m_{S/G}$ [TeV]	[0.26–3.00]	[0.50–3.00]	[0.26–1.00]	[0.26–0.50]	[0.26–1.00]	[0.26–0.50]

- Upper limits at 95% CL on the cross-section of the ggF non-resonant SM HH production as a function of κ_λ (=λ/λ_{SM}).

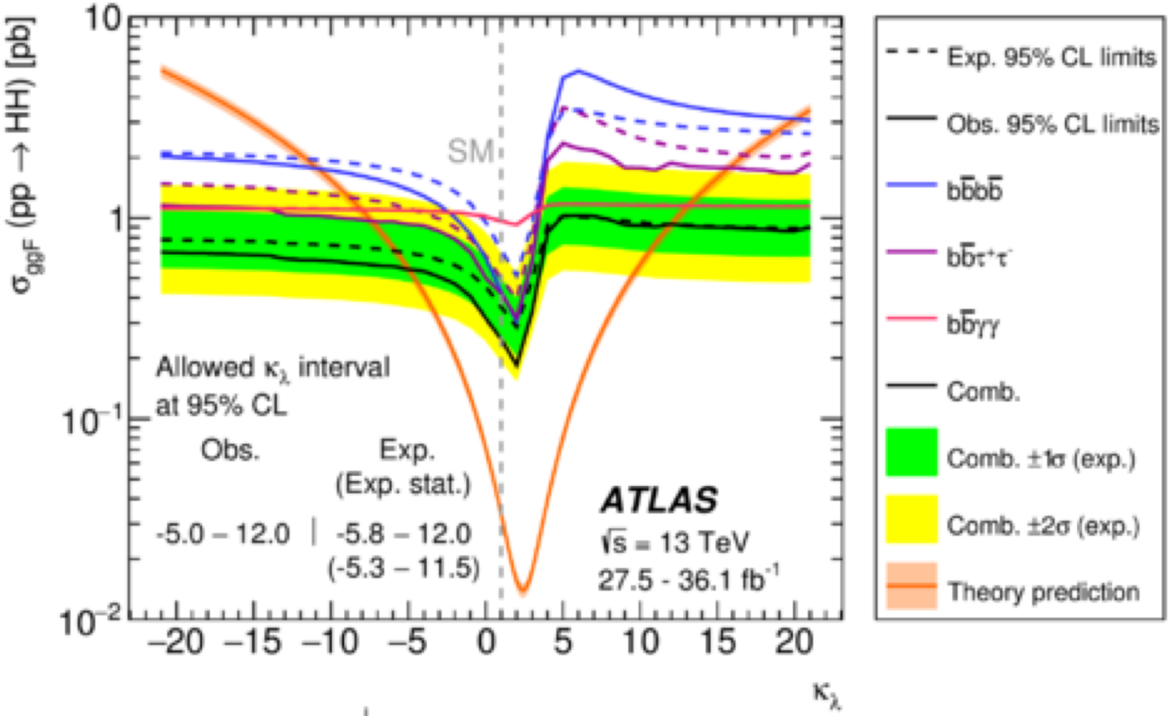

Final state	Allowed κ_λ interval at 95% CL Obs.	Exp.	Exp. stat.
$b\bar{b}b\bar{b}$	−10.9 — 20.1	−11.6 — 18.8	-9.8 — 16.3
$b\bar{b}\tau^+\tau^-$	−7.4 — 15.7	-8.9 — 16.8	-7.8 — 15.5
$b\bar{b}\gamma\gamma$	−8.1 — 13.1	-8.1 — 13.1	-7.9 — 12.9
Combination	−5.0 — 12.0	-5.8 — 12.0	-5.3 — 11.5

Limits on spin-0 heavy scalar cross-sections

Run 1:

CMS measurements & ATLAS combination

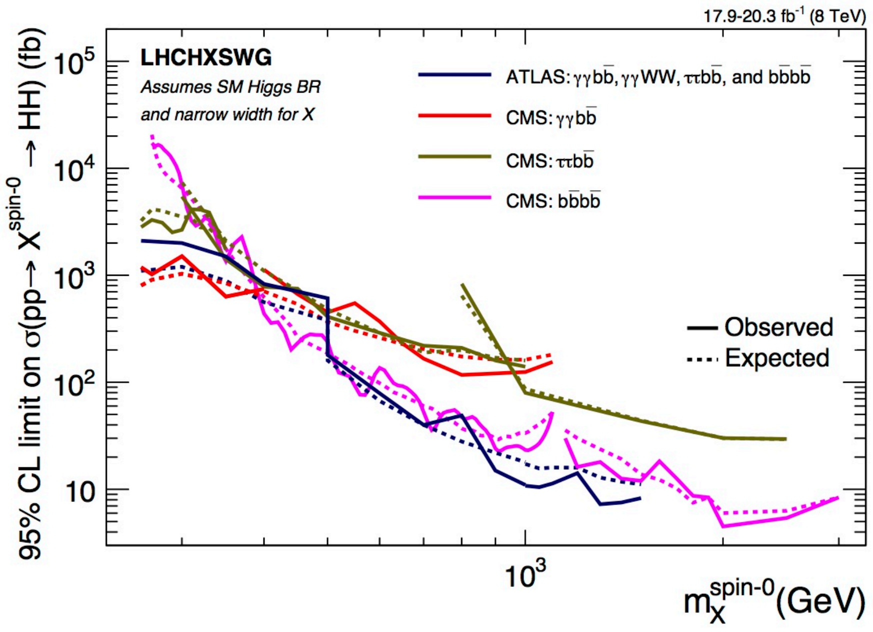

Run 2:

ATLAS 2019 combination

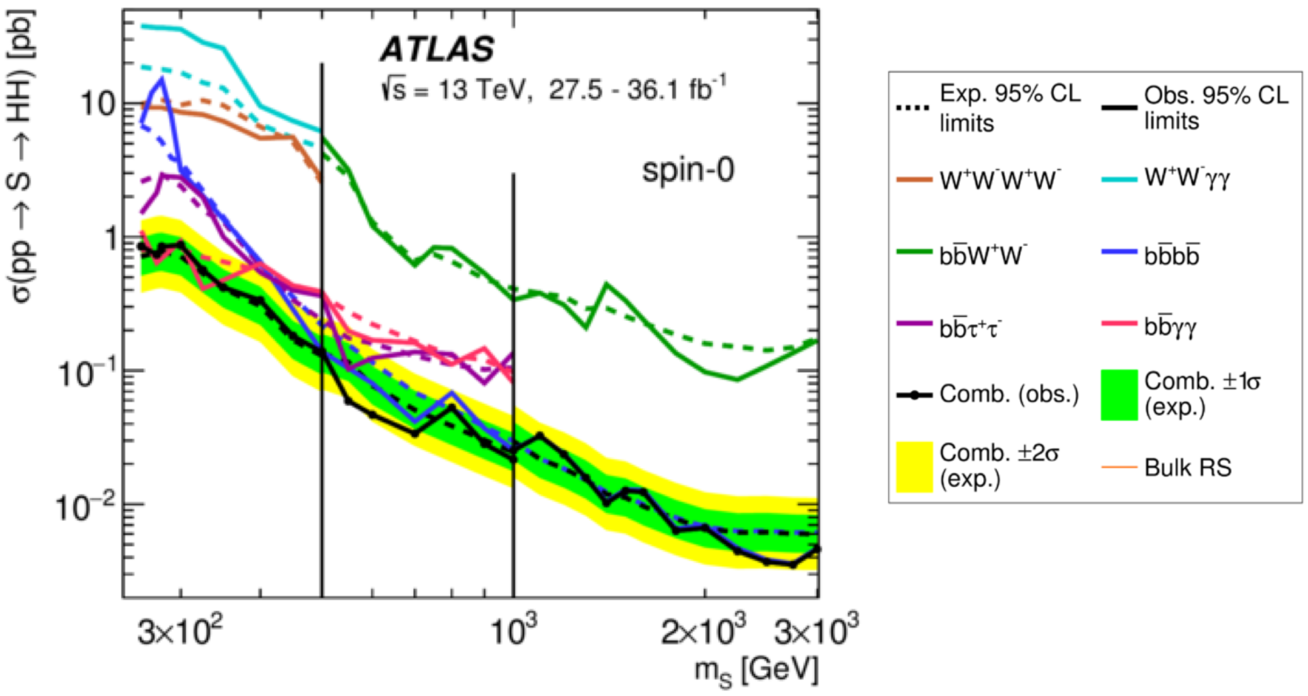

Improvements due to: larger cross-sections (31fb vs 10 fb), luminosity (36.1/fb vs 17.9/fb), experimental reconstruction

Search for non-resonant Higgs boson pair production bb lvlv channel

- bb+WW/ZZ/$\tau\tau$ final states
- main backgrounds: Top and Z/$\gamma*$ + jets processes ,
- signal selection
  - $m_{ll}\in(20,60)$ GeV and
  - $m_{bb}\in(110,140)$GeV
- DNN classifier trained on HH→bbWW* events
- The classifier produces four outputs

p_i (i∈ {HH,Top,Z-ll,Z-ττ}).

- The main discriminant $d_{HH}=\ln[p_{HH}/(p_{Top}+p_{Z-ll}+p_{Z-\tau\tau})]$.

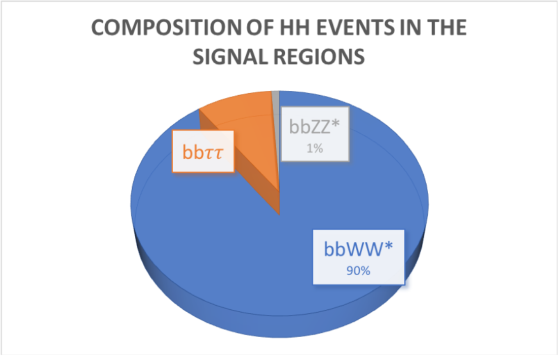

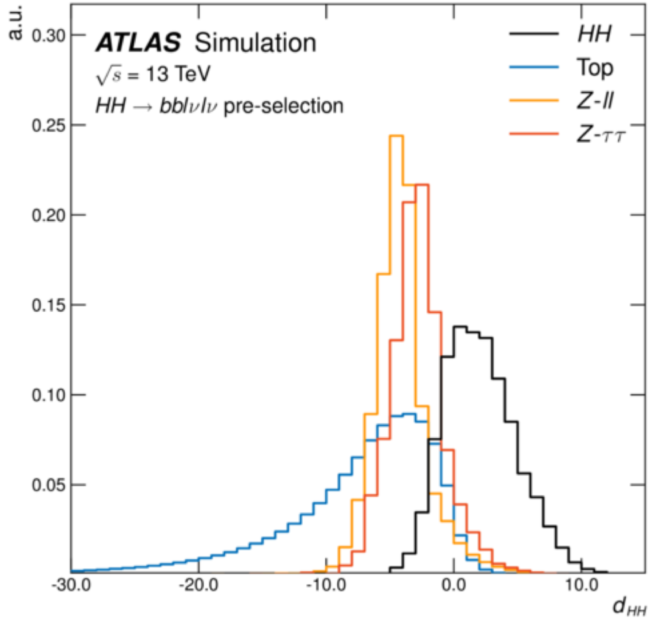

	-2σ	-1σ	**Expected**	$+1\sigma$	$+2\sigma$	**Observed**
$\sigma(gg \to HH)$ [pb]	0.5	0.6	0.9	1.3	1.9	1.2
$\sigma(gg \to HH)/\sigma^{SM}(gg \to HH)$	14	20	29	43	62	40

Conclusions

- New di-boson measurements at the LHC crucial to fully explore the SM SU(2)xU(1) symmetry structure and EW symmetry breaking
  - ATLAS studies move from first observations of rare EW processes to precision measurements
  - Numerous constraints on New Physics in anomalous couplings and using the SMEFT framework
- Interplay between SM and Higgs measurements are starting to be explored through measurements of four leptons invariant mass spectra and EFT fits
- Di-Higgs searches performed in several channels
  - SM Higgs production not yet observed
  - Limits on the Higgs trilinear coupling largely improved
  - Exclusion limits on BSM resonances
- Most measurements statistically limited; improvements are expected at Run3 and HL-LHC
- Extensive work, challenges and opportunities ahead to collect quality data and produce good physics results

Backup

rapidity and pseudorapidity

rapidity

$$y = \frac{1}{2} \ln \frac{E + p_z c}{E - p_z c},$$

pseudorapidity

$$\eta \equiv -\ln\left[\tan\left(\frac{\theta}{2}\right)\right]$$

$$\eta = \frac{1}{2} \ln\left(\frac{|\mathbf{p}| + p_{\mathrm{L}}}{|\mathbf{p}| - p_{\mathrm{L}}}\right)$$

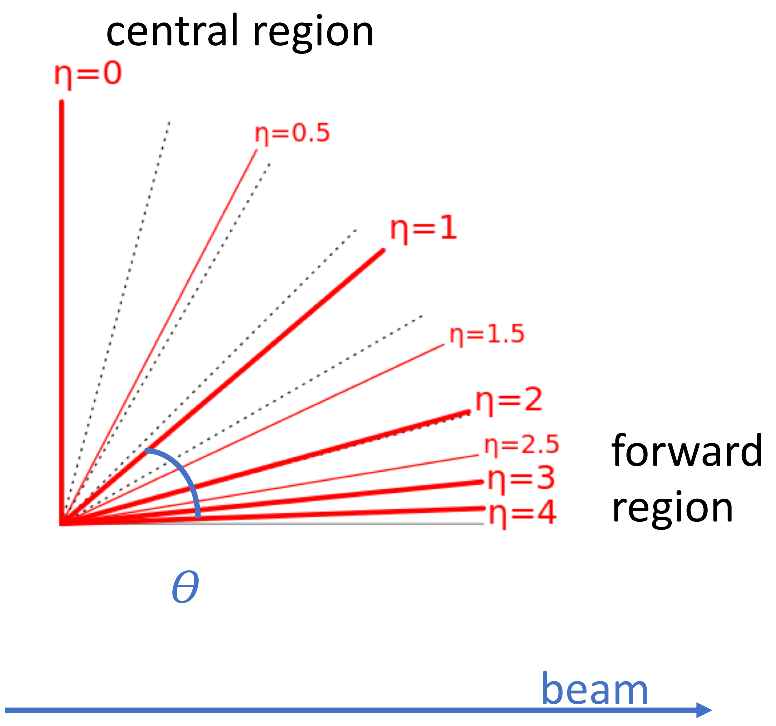

In the limit m→ 0 η→ y